Safety Evaluation of Bridge Scour by Fluid-Structure Interaction

Tzu-Kang Lin,[1] Po-Wei Chen,[2] Hao-Tun Chang,[3] and Kuo-Chun Chang[4]

[1]Department of Civil Engineering, National Yang Ming Chiao Tung University, No. 1001, Daxue Road, East District, Hsinchu City, 300093, Taiwan (R.O.C.);
e-mail: tklin@nctu.edu.tw Corresponding author.
[2]Department of Civil Engineering, National Yang Ming Chiao Tung University, No. 1001, Daxue Road, East District, Hsinchu City, 300093, Taiwan (R.O.C.);
e-mail: e2171918@gmail.com
[3]Department of Civil Engineering, National Yang Ming Chiao Tung University, No. 1001, Daxue Road, East District, Hsinchu City, 300093, Taiwan (R.O.C.);
e-mail: happy90069harry@gmail.com
[4]Department of Civil Engineering, National Taiwan University, No.1, Sec. 4, Roosevelt Road, Da'an District, Taipei City, 106319, Taiwan (R.O.C.);
e-mail: ciekuo@ntu.edu.tw

ABSTRACT

A finite element simulation was conducted in this study to correctly evaluate the effect of fluid by developing a fluid–solid interaction (FSI) system. In the FSI system, simulation results for both the fluid and solid systems were exchanged. Thus, the force generated by the fluid system could be incorporated into the solid system to estimate the dynamic response of a pier. A scaled single-pier scour test was first conducted numerically and experimentally. The results showed that the established FSI system can consider the fluid–solid interaction and reflect pier scour behavior accurately. To test the validity of the proposed system, the scour process was numerically conducted on an engineering bridge. Two safety factors were proposed to evaluate the stability of the bridge structure under extreme events such as rainfall or typhoon. The result has proven the scour stability of the bridge pier can be appropriately evaluated by the proposed system.

1. INTRODUCTION

A survey conducted in the United States indicated that approximately 60% of bridge failures are attributed to hydraulic activity, and that only 3% of such failures are attributed to seismic activity [1]. Scour, classified as a hydraulic activity in the survey, is caused by the loss of bed material near the piers due to the water flow. A bridge stability and scour assessment indicated that scouring of piers in rivers can be classified into three types according to its cause and position: degradational, contraction, and local scour [2]. Degradational scour occurs gradually over time due to floods or some human activities. The occurrence of contraction and local scour is directly related to the bridge structure. The flow velocity near a bridge increases because of the corresponding abutments and piers, resulting in a contraction scour in the riverbed. Among these three types of scour, local scour results in erosion of bed material near the piers due to the generated vortices and poses the greatest threat to the bridge structure.

Studies have shown the effect of scour on bridge foundation performance such as stability and bearing capacity. Prendergast *et al.* [3] developed numerical and practical scaled pile models. Analyzing the response of the models after excitation by an impulse force revealed a loss of structural natural frequency and occurrence of scour at the foundation of the piles. A lower dominant frequency was considered to imply a lower constraint, suggesting a weakened structure. Prendergast *et al.* [4] studied the natural frequency response of structure, and Tseng *et al.* [5] performed numerical simulations on the piers of offshore wind turbines, concluding that the natural frequency decreased, and the deformation increased with the loss of riverbed materials near the piers.

The flow behavior of water near piers, especially piers with scour, is highly nonlinear where the velocity fields change with time and distance from the piers. Normally, the effects of fluid behavior may be smaller than those of live and dead loads on a bridge. However, bridge failure may occur because of overestimation of stability in areas subjected to severe scour. Considering the existing regulations and the complexity of structural design, fluid behavior is typically simplified as a linear distribution in most structural design procedures. Therefore, a method in which both structural and fluid conditions are considered is required to accurately evaluate the stability of bridge structures under the influence of current forces. An FSI system was conducted in this study to correctly evaluate the effect of fluid–solid interaction. The result of the scaled single-pier scour test showed that the proposed FSI system can consider the non-linear dynamic interaction and reflect accurate pier scour behavior. Two safety factors were then proposed to evaluate the stability of bridge structure under extreme events. The results can serve as a reference in establishing guidelines for bridge.

2. METHODOLOGY

To analyze the stability of the bridge by considering the influence of the fluid, two methods including FSI and Short-Time Fourier Transform (STFT) were applied. These methods are described as follows.

2.1 FLUID-SOLID INTERACTION MODEL

The numerical model consist of a transient structural system and a fluid flow system, where the boundary conditions of these two models are influenced by each other. Thus, by using the fluid-solid interaction model, the response of bridge under the influence of fluid can be simulated. As depicted in Figure 1, the responses of the transient structural and fluid flow modules were connected through system coupling in the simulation. In the solid module, the external force was applied, and the structural displacement was the output. In the fluid module, the geometric shape of the flow field was generated with the structural displacement as the boundary condition, and the fluid behavior was the output. Some important settings for the sophisticated model are listed as follows:

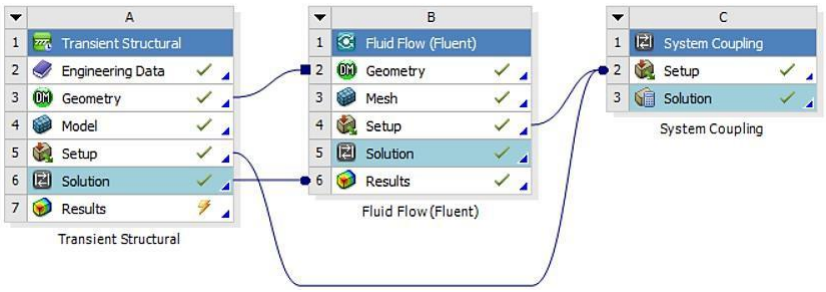

Figure 1. System coupling for FSI simulation.

2.2 SOIL MODEL

Generally, the soil is compressible and does not have a specific volume, which renders the simulation of earth pressure in the numerical model difficult. Solid element proposed by Chiroux *et al.* [6] discrete element method (DEM 1989) proposed by John *et al*. [7], and the soil spring proposed by Prendergast *et al*. [3]have been applied to simulate reaction forces in soil. To achieve accurate results, the solid element and DEM require details of the properties of soil. Considering the number of soil parameters required as well as the model complexity, a relatively simplified model, soil spring, was applied in this study. According to the current code in Taiwan [8], the setting of the soil spring in the numerical model is illustrated in Figure 2.

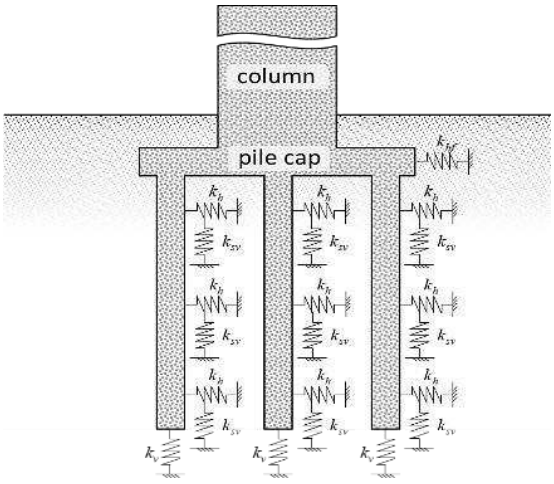

Figure 2. Setting of the soil spring in the numerical model.

The stiffness of the soil springs set horizontally on a pile is expressed as [8]

$$k_h = 0.34(\alpha E_0)^{1.10} D^{-0.31} (EI)^{-0.103} \quad (1)$$

where α is the modulus of the seismic subgrade reaction, and E_0 is the modulus of the subgrade deformation. The modulus of the subgrade deformation can be further defined by the *N* value from the standard penetration test (SPT) as

$$E_0 = 28N \quad (2)$$

where *D*, *E*, and *I* are the diameter, Young's modulus, and second axial moment of the area of the pile structure, respectively. For the modulus of the seismic subgrade reaction, α is typically set to 2 considering the seismic event. In this study, the influence of earthquakes was not included; therefore, α was set to 1.

The stiffness of the soilsprings set vertically on the pile can be described as [8]

$$k_{sv} = 0.3k_h \tag{3}$$

2.3 SHORT-TIME FOURIER TRANSFORM

Fourier transform is generally applied to discrete signals and can be expressed as

$$X[\omega] = \sum_{n=-\infty}^{\infty} x[n]e^{-i\omega n} \tag{4}$$

where *n* is the discrete step in the time domain, and ω is the frequency content after transform. During the scour test, the embedded depth decreased because of the loss of bed elements, leading to a nonconstant model boundary condition. Therefore, short-time Fourier transform (STFT), a method that can be used to analyze the time-frequency domain, was applied and can be expressed as

$$X[m, \omega] = \sum_{n=-\infty}^{\infty} x[n]w[n - w]e^{-i\omega n} \tag{5}$$

where *n* represents the time point; ω represents the frequency; m expresses the time delay, and *w* is the window function that shifts along the time domain. Changes in modal dynamic features with time can be obtained using the window function. To improve the STFT performance, a Hamming window is adopted as

$$w[n] = 0.53836 - 0.46164\cos\left(\frac{2\pi n}{N-1}\right) \tag{6}$$

where N is the data points of the window length.

3. PRACTICAL APPLICATION

A practical bridge, the Shi-Bin Bridge, was further considered for scour stability assessment. This bridge is one of the most important bridges in Taiwan, as it connects two major counties by crossing over the Zhuoshui River. To protect the bridge from erosion and scour by the river, it is necessary to investigate the health condition of the structure. Therefore, the Shi-Bin Bridge was selected for scour monitoring.

The Shi-Bin Bridge was built in July 1991. This bridge is 2730 m long, and its clear width is 18 m. The bridge is composed of 78 spans, and each span is 35 m long. As shown in Figure 3, the Shi-Bin Bridge comprises a four-lane original bridge and a pair of two-lane extension bridges. With a three-column design as the pier, the original four-lane bridge supports decks with seven simply support Precast Concrete-I (PCI) girders. Totally 36 piles in a group are connected to a 2-m-thick pile cap, and each pile is 33 m long. For the extension bridge, the single-column pier supports decks with four simple support PCI girders. A group of 20 piles is connected to a 2-m-thick pile cap where each pile is 33m long.

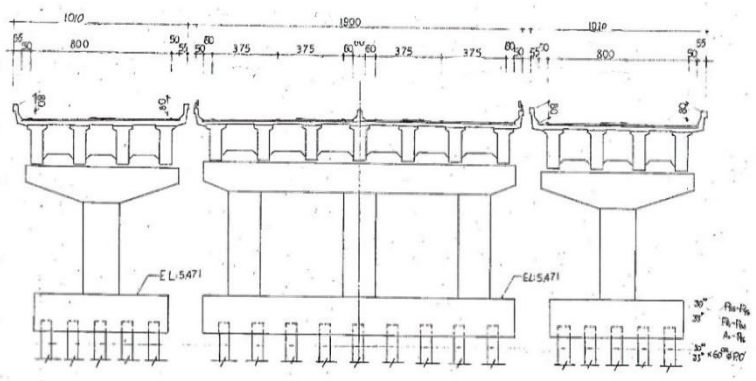

Figure 3. Cross-sectional view of the Shi-Bin bridge.

According to the as-built drawing, each pier of the extension bridge bears a total weight of 558 tons, including the pier, column, cap, beam, PCI girders, and deck plate. The weights of the deck, PCI girder, and vehicle were transferred through the cap, beam, and column to the foundation of the pier structure. As the compressive strength of the prestressed beams of 350 kgf/cm^2 and a unit weight of 2400 kg/m^3 was used on the bridge abutments, pier columns, and deck plates, the total mass should be deducted 113 tons by calculation. Thus, the mass of PCI girders and deck, totally 445 tons per pier, was set at the top of the cap beam.

3.1 FSI SIMULATION

As shown in Figure 4(a), the model of the Shi-Bin bridge including the cap, beam, column, pile cap, and pile was established according to the geometric design of the bridge. To simplify the connection between the pier and piles, the hollow concrete pile of the bridge was replaced by a solid concrete piles. Moreover, the soil springs were set in the current direction, driving direction, and under pile. Thus, the stability of this model can be supported by the soil springs. The vibration data in the current direction were applied to obtain the dynamic properties of the pier, which involved a fundamental frequency of 2.34 Hz. The N value was set to 25 to define the stiffness of the soil spring in this study. Regarding the setting of soil springs, four soil springs were evenly set in vertical direction under the foundation. Moreover, both in the longitudinal and transversal direction, soil springs were set every 1 m in the vertical direction according to the group pile design of the foundation. Thus, the soil springs were placed in an array to enhance stability in the numerical model as shown in Figure 4(b)

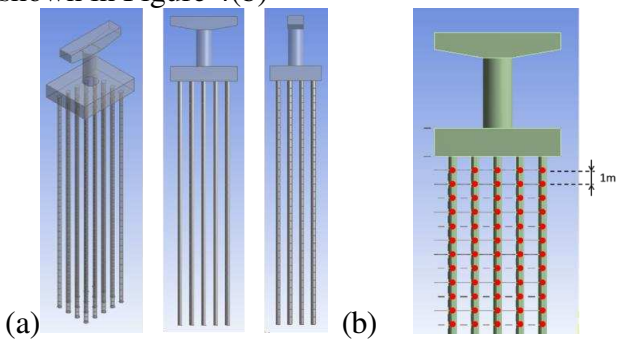

Figure 4. Numerical model of the Shi-Bin Bridge.
(a) Column and piles. (b) Arrangement of soil springs.

A linearly increasing flow velocity was applied to the inlet boundary condition to avoid simulation failure. Two free-decay signals were observed with the displacement of the pile top along the current direction. To define the structural displacement at the top of the pile under different scour and flow velocity conditions, the mean displacement was calculated as the displacement index in the steady state.

The fluid behavior reflecting the down flow, horseshoe vortex, and wake vortex under each boundary condition could be obtained from the simulation results. For the 10-m scour depth and 2-m/s flow velocity, down flow was observed at the bottom of the column and near the pile foundation. This flow, which was parallel to gravity, was engendered by the obstacle near the pile cap.

Figure 5 depicts the distribution of the flow velocity at the transversal section. The velocity on the top is about 3.939 m/s, and horseshoe vortices occurring near the bottom of the column can be observed. The horseshoe vortices usually form around obstacles such as the bridge pier in the flowing water. Scouring of the riverbed may be caused by horseshoe vortices from both upstream and downstream of the pier.

Meanwhile, the vortices occurring near the pile changed with time and distance from the riverbed, indicating that these vortices could be classified as wake vortices. Although the vortices at the transversal section were not generated from the down flow, the riverbed material near this position was eroded, thus causing scouring.

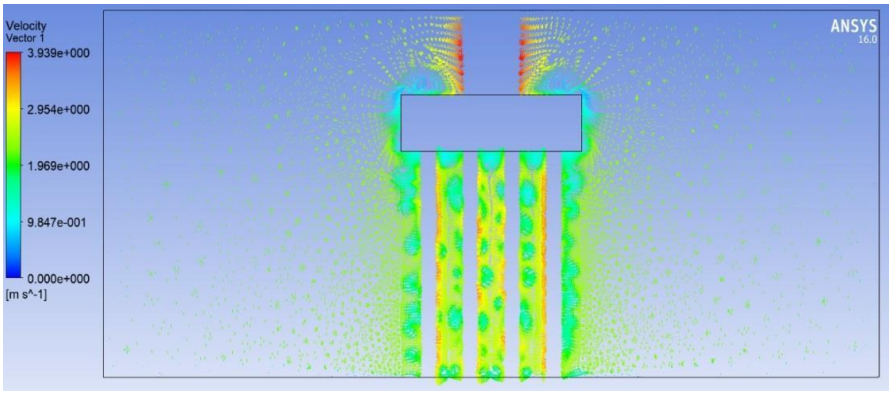

Figure 5. Distribution of flow velocity at the transversal section.

3.2 STABILITY EVALUATION

The FSI simulation, which considered a more integrated fluid behavior, indicated a large structural displacement at the pile top. Compared with the pile cap, column, cap beam, and other bridge elements with higher stiffness, the pile of a bridge has a small diameter, which may be a vulnerable characteristic in the bridge structure. In this study, the allowable displacement and ultimate moment of the piles were applied to evaluate the stability of the bridge.

Excessive pile displacement may cause a threat to road users. Furthermore, the P-Δ phenomenon, which can cause column failure, cannot be ignored for pile elements with a slender geometric design. The stability factor [9] of a pile can be defined as

$$Q_s = \frac{P\Delta_0}{VL_C} \tag{7}$$

Where P and V are the axial force and shear force applied to the pile, respectively; Qs, Δ0, Lc, and Mu are the stability factor, relative displacement at the pile top, length of the pile, and ultimate moment of the pile, respectively. According to the mentioned regulation, a stability threshold of 0.25 should be set.

The allowable displacement can then be derived as

$$\Delta_0 = Q_s = \frac{VL_C}{P} = Q_s \frac{M_u}{P} \tag{8}$$

Therefore, the allowable displacement under a specific axial loading condition can also be defined by examining the ultimate moment of the pile element from a P–M interaction diagram. On the basis of the allowable displacement and ultimate moment, two safety factors, namely, the safety factor based on displacement (SFdis) and safety factor based on moment (SFmoment) are proposed as

$$SF_{dis} = \frac{\Delta_0}{\Delta} \tag{9}$$

$$SF_{moment} = \frac{M_u}{M} \tag{10}$$

where Δ and M are the displacement at the pile top and moment at the pile, respectively.

Figure 6 shows the simulated axial stress distribution on the pile with the embedded depth of 12m. The positive maximum axial stress is about 116.54 ton/m2, and the negative maximum axial stress is 117.55 ton/m2. As shown in the figure, the blue color indicates that the minimum axial stress occurs on the soil surface. The stress is increased gradually along the vertical direction to the pile cap, and the maximum axial stress is expressed in yellow color. The maximum axial forces calculated by different flow velocity and scour depth are shown in Table 1. Among them, the scour depth is calculated based on the elevation of the top of the pile cap being 0 meters.

When the scour depths are 0 meters and 2 meters, the top of the pile cap are restricted by soil springs. Thus, the safety factor cannot be calculated according to the relative displacement between the pile top and the riverbed. Therefore, only the axial force value of the erosion depth below 4 meters is listed in Table 1.

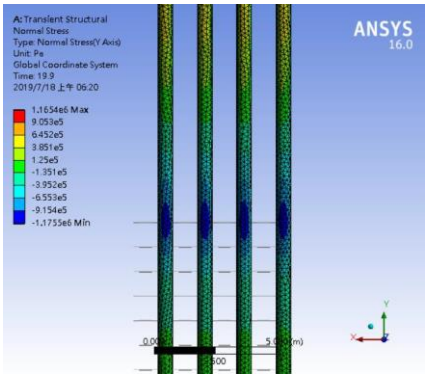

Figure 6. The simulated axial stress distribution on the pile

Table 1. The maximum axial force of fluid-solid interaction. (N)

Scour depth(m)	Flow velocity(m/s)					
	0.5	1.0	1.5	2.0	2.5	3.0
0	-	-	-	-	-	-
2	-	-	-	-	-	-
4	53413.85	53416.30	53419.47	53384.74	53324.93	53304.01
6	53927.74	53901.52	53892.26	53828.94	53749.19	53690.11
8	54856.68	54838.10	54843.56	55132.36	54783.61	54680.72
10	55701.01	55695.67	55667.72	55629.97	-	-

The threshold values of 3 and 2 were set for alert and action decisions, and the derived safety factors are listed in Table 2. The FSI simulation was conducted, and safety factors were obtained as presented in Table 2. The combinations marked in yellow and red represent values lower than 3 and 2, respectively. For example, for the ultimate moment method, the safety factor met the alert threshold when the flow velocity was 3 m/s and the scour depth was 16 m. The action threshold was further triggered when the scour depth reached 18m. Meanwhile, by considering the allowable displacement method under the same flow velocity of 3 m/s, the safety factors met the alert and action thresholds while the scour depths were 20 m and 22 m, respectively. The result shows that the safety factors are controlled by the ultimate moment. Both methods can provide a rapid and easy method to evaluate the scour stability under extreme events.

Table 2: Safety factors for different scour and flow velocity conditions.

(a) Allowable displacement method

Velocity / depth	0.5	1	1.5	2	2.5	3
0	-	-	-	-	-	-
2	-	-	-	-	-	-
4	5318	2825	1730	1167	836.3	607.5
6	1697	806.8	463.4	315.3	222.4	161.9
8	592.9	283.9	165.7	113.0	80.6	58.2
10	305.3	139.8	93.4	59.9	38.6	27.9
12	172.8	76.7	48.6	31.7	20.9	15.1
14	106.2	46.0	29.5	19.1	12.4	8.9
16	69.7	29.6	19.1	12.3	7.9	5.7
18	48.0	20.0	13.1	8.4	5.3	3.8
20	34.4	14.1	9.3	5.9	3.7	2.7
22	25.5	10.3	6.8	4.3	2.7	1.9
24	19.3	7.7	5.1	3.2	2.0	1.4
26	15.0	5.9	3.9	2.5	1.5	1.1
28	11.9	4.6	3.1	1.9	1.2	0.8
30	9.5	3.7	2.5	1.5	0.9	0.6

(b) Ultimate moment method

Velocity / depth	0.5	1	1.5	2	2.5	3
0	-	-	-	-	-	-
2	-	-	-	-	-	-
4	996.9	1350	482.5	265.4	172	118.2
6	554.2	220.2	116.4	74.2	51.8	37.3
8	231.4	92.8	56.8	38.5	27.1	18.5
10	343	68.4	43.7	26.2	14.2	9.9
12	198.4	28.8	22.1	14.7	8.7	6.0
14	159.8	17.3	14.6	9.9	5.7	4.0
16	132.5	11.1	10.2	7.0	4.0	2.8
18	112.3	7.5	7.4	5.2	2.9	2.0
20	96.8	5.3	5.6	4.0	2.2	1.5
22	84.7	3.8	4.3	3.1	1.7	1.2
24	74.9	2.8	3.4	2.5	1.3	0.9
26	67.0	2.2	2.7	2.0	1.1	0.7
28	60.3	1.7	2.2	1.7	0.9	0.6
30	54.8	1.3	1.9	1.4	0.7	0.5

4. SUMMARY AND CONCLUSIONS

This study conducted a FSI simulation to evaluate the scour stability of bridge piers. A feasibility assessment was first conducted to evaluate the applicability of the proposed FSI model; small errors were observed between the scaled pier scour experiment and numerical simulation in the frequency domain, demonstrating the feasibility of the

method. The proposed FSI model was subsequently applied to simulate the fluid behavior around a bridge structure subjected to scour. Both FSI and static simulations were implemented under different scour depths and flow velocity conditions, and the structural displacements of the pile top were noted. According to the simulation results, a larger structural displacement was observed in the FSI simulation, indicating that the constant applied in the current force calculation may result in an underestimation of the scour effect. By using the P–M interaction diagram of the pile element, two safety factors based on the allowable displacement and ultimate moment were proposed. Finally, the critical scour depth for different flow velocities can be rapidly determined according to the alert and action thresholds. In practical application, the boundary condition setting of the FSI model and the balance between the element size and the time spending on simulation should be carefully considered to ensure the performance of the proposed system. The results can serve as a reference in establishing guidelines for bridge and traffic control for preventing disasters and evacuating people during the occurrence of floods.

REFERENCES

[1] A. M. Shirhole and R. C. Holt, "Planning for a comprehensive bridge safety program," *Transportation Research Record*, Washington, DC: Transportation Research Board, National Research Council. no. 1290, 1991.

[2] G. W. Parker, L. Bratton and D. S. Armstrong, "Stream stability and scour assessments at bridges in Massachusetts," *Report Marlborough*, Massachusetts- Rhode Island Water Science Center. no. 97-588, 1997.

[3] L. J. Prendergast, D. Hester, K. Gavin and J. J. O'Sullivan, "An Investigation of the Changes in the Natural Frequency of a Pile affected by Scour," *Journal of sound and vibration*, vol. 332, no. 25, pp. 6685-6702, 2013.

[4] L. J. Prendergast, K. Gavin and P. Doherty, "An investigation into the effect of scour on the natural frequency of an Offshore Wind Turbine," *Ocean Engineering*, no. 101, pp. 1-11, 2015.

[5] W. C. Tseng, Y. S. Kuo, K. C. Lu, J. W. Chen, C. F. Chung and R. C. Chen, "Effect of Scour on the Natural Frequency Responses of the Meteorological Mast in the Taiwan Strait," *Energies*, vol. 11, no. 823, pp. 1-18, 2018.

[6] R. C. Chiroux, W. A. Foster Jr., C. E. Johnson, S. A. Shoop and R. L. Raper, "Three-dimensional finite element analysis of soil interaction with a rigid wheel," *Applied Mathematics and Computation*, no. 162, pp. 707-722, 2005.

[7] M. T. John, T. C. Brent, R. K. Claudia and G. Carlo, "Discrete Numerical Model For Soil Mechanics," *Journal of Geotechnical Engineering*, vol. 115, no. 3, pp. 379-398, 1989.

[8] Design Specifications of Highways and Bridges, Ministry of Transportation and Communications; Taipei, Taiwan, 2009.

[9] Kármán, Th. von. "Uber den Mechanismus des Widerstandes, den ein bewegter Körper in einer Flüssigkeit erfährt," *Nachrichten von der Gesellschaft der*

Wissenschaften zu Göttingen, Mathematisch-Physikalische Klasse, pp. 509- 517, 1911